NorthWest Research Associates, Inc.
P.O. Box 3027 • Bellevue, WA 98009

NWRA-CR-91-R074 13 December 1991

Final Report Covering the Period 27 September 1990 through 26 September 1991

REPORT ON THE SEARCH FOR ATMOSPHERIC HOLES USING AIRS IMAGE DATA

Prepared by
Lee A. Reinleitner

Prepared for
NASA Headquarters
Washington, DC
Scientific & Technical Information Facility
Grant No. NASW-4535

300-120th Ave. N.E. • Suite 220, Building 7 • Bellevue, WA 98005 • (206) 453-8141 • FAX (206) 646-9123

NWRA-CR-91-R074 13 December 1991

Final Report Covering the Period 27 September 1990 through 26 September 1991

REPORT ON THE SEARCH FOR ATMOSPHERIC HOLES USING AIRS IMAGE DATA

Prepared by
Lee A. Reinleitner

Prepared for
NASA Headquarters
Washington, DC
Scientific & Techincal Information Facility
Grant No. NASW-4535

REPORT ON THE SEARCH FOR ATMOSPHERIC HOLES USING AIRS IMAGE DATA

I. INTRODUCTION

In 1986 an unusual set of data anomalies in the DE-1 image data was reported by Frank *et al* [1986]. These anomalies consisted of single-pixel intensity decreases in the images of the earth's dayglow emissions at vacuum-ultraviolet (VUV) wavelengths, primarily those of atomic oxygen at 130.4 nm. These dark spots, or atmospheric "holes," have been interpreted by Frank *et al* [1986] to be the result of VUV absorption by water vapor resulting from the tidal disruption and vaporization of small bodies of ice with approximately 100 metric tons mass and extremely low density. These low-density ice bodies often have been referred to as mini-comets or small comets. The resulting vapor cloud from these small comets' disintegration would be on the order of 50 km in diameter and above the upper ionospheric region (200 to 300 km) where photoelectrons produce the VUV dayglow background. These falling clouds would eventually impact and dissipate in the upper atmosphere, but before doing so would block out the VUV dayglow background as observed by a satellite imager. In addition to the DE-1 satellite, using the images on the Viking satellite, Frank *et al* [1989] claimed to have observed pixel intensity reductions of a type predicted by the small-comet hypothesis, though the size of the data set was very limited, and the results are subject to debate [Cragin, 1990].

Streaks observed by Yeates [1989], having the characteristics of these small comets, have kept this controversial topic open. These streaks were observed with the Spacewatch Telescope at Kitt Peak and a CCD detector when the telescope was slued across the sky to match the predicted motion of the small comets, but they are not widely acknowledged as convincing proof of the hypothesis [Kerr, 1989].

Controversy continues in the scientific community regarding the implications of the required influx rate for these mini-comets to produce the observed atmospheric holes [Chubb, 1986 (and reply); Cragin *et al*, 1987 (and reply); Davis, 1986 (and reply); Donahue, 1986 (and reply); Hanson, 1986 (and reply); McKay, 1986 (and reply); Morris, 1986 (and reply); Nakamura and Oberst, 1986 (and reply); Rubincam, 1986 (and reply); Soter, 1987 (and reply), Wasson and Kyte, 1987 (and reply); Dessler (1991) (reply pending)]. The influx rate required for the observed frequency of the atmospheric holes is about 20 per minute over the entire surface of the earth, and such an influx would have major implications for the geological evolution of the planet.

Examination of a data set from another instrument, having imaging capability in the far-VUV range, for evidence either supporting or weighing against the small-comet hypothesis, would be highly desirable. The Auroral Ionospheric Remote Sensor (AIRS) is an instrument with this capability. This report will not delve into the various arguments for or against the small-comet hypothesis advanced by Frank *et al* [1986]. Its exclusive focus will be an examination of the AIRS data to search for evidence either for or against the existence of atmospheric "holes."

II. BACKGROUND

The AIRS instrument was flown on the Polar BEAR satellite, which carried a complement of interrelated experiments designed for auroral and ionospheric observations, and was the third in a series of satellite missions sponsored by the Defense Nuclear Agency of the US Department of Defense. It is a three-axis gravity-gradient stabilized platform, which was launched on November 13, 1986. It is in a nearly circular polar orbit with an inclination of ~90 degrees and an altitude of approximately 1000 km. The orbital period is approximately 110 minutes, with a 27-minute period of on-time over the northern polar cap. The Polar BEAR spacecraft construction began with extensive modification of a Navy Navigation Satellite System (NNSS) spacecraft, Oscar 17, which had been on display in the Smithsonian Air and Space Museum. Modifications and additions to the satellite were performed by the Applied Physics Laboratory at Johns Hopkins (APL). The AIRS instrument was built for the Air Force Geophysics Laboratory by APL.

The accumulated data were not stored on the satellite, but were downlinked directly to one of several receiving stations. Data were received only during periods that the satellite signal was received directly on the ground from one of the receiving stations. During a pass over a receiver, all telemetry information that the satellite produced was transmitted to the receiver for a period lasting for up to 12.5 minutes. Three fixed-receiver stations were located at Tromso, Norway; Sondre Stromfjord, Greenland; and Churchill, Canada. An additional transportable receiver (ROVER) usually was based in Bellevue, WA, but has been stationed at various locations around the world.

The AIRS instrument was a single-photon detection instrument with a sensitivity of about 50 Rayleigh/count for VUV channels and approximately 1000 Rayleigh/count for near-UV/visible channels. It was designed as a multi-mode instrument, which had a four-channel system to operate simultaneously in the VUV, near-UV, and visible spectral bands. Two of the data channels used a spectrometer with a 3.6-nm bandpass to provide total coverage from 115.0 nm to 180.0 nm in the VUV range. The other two channels utilized a filter selector system to provide preselected 1.0 nm bandwidth spectral channels at 337.1 nm, 391.4 nm and 630.0 nm, with a 20.0-nm wide channel centered at 225.0 nm. All four channels viewed the image below the spacecraft via appropriate optics and a scan mirror system. Although the instrument could be used in either spectrometer, photometer, or imaging modes, only the imaging mode data were used for this study. Further information concerning the various modes and capabilities is available from Schenkel and Ogorzalek [1987] and Schenkel *et al* [1986].

When in the imaging mode, a mirror system scanned a line across the orbital plane of motion (perpendicular to the motion of the satellite), and thus an image was built up as the satellite moved along its orbital path. (See Figure 1, taken from Schenkel and Ogorzalek [1987].) The satellite has a forward orbital velocity of approximately 6.6 km/sec at the satellite-ground subtrack point. The line-scan duration and the equivalent forward motion of one line width were made approximately equivalent, to provide nearly contiguous image scans. The image system thus scanned +/-67.2 degrees in 2.36 seconds with a 0.64-second retrace for a total line-scan period of 3.0 seconds. Actual image line-scan data are collected over only +/65.2

degrees for a total of 326 pixels per scan line. (See Figure 1.) The total number of scan lines per image varied (up to a maximum of 250), depending on how long the satellite was over a receiver. All four simultaneous channels were optically co-aligned. The image-pixel distortion increased with the off-nadir viewing angle, although that had little effect on this study. Since AIRS used a stepper motor rather than the rotation of the satellite (as was the case in DE-1), each pixel had an accumulation time of 6.83 msec with a pixel dwell time of 7.03 msec. In addition, the VUV channels were designed to provide approximately 25% overlap in the direction of the spacecraft orbit. In the image scan-line direction, the pixel width was 0.373 degrees, with 0.40 degrees between pixel centers. Immediately after the accumulation time of 6.83 milliseconds, the pixel counts were converted into a "packed" form (8 bits) and stored until transmitted to the ground receiver. The formula for conversion of the packed bits to unpacked integer pixel counts is:

$$\text{Counts} = (2^{\text{exponent}} \times (\text{mantissa} + 32)) - 32$$

where the most significant three bits form the exponent and the least significant five bits form the mantissa. Note that this compressed format allows a range of 0 to 8032 counts to be stored in a quasi-logarithmic form. Since the pixel dwell time was so much shorter than the scan-line period, the data was stored on the satellite in packed form most of the time.

Since the Polar BEAR satellite was in a low-altitude (1000 km) circular orbit, which provided AIRS with a 6.5-km by 26.7-km resolution on the ground at nadir, it should be possible to resolve the postulated (~50 km diameter) water-vapor cloud against a dayglow background. Due to the scanning method of the AIRS imager, the anticipated signature is a series of pixel-intensity reductions in one scan line, as shown in Figure 2. Although Frank *et al* [reply to Chubb, 1986] presented evidence of adjacent pixel decreases on one scan line, this was unusual for DE-1 due to its limited amount of time near perigee. Polar BEAR was at low altitude (1000 km) at all times, so all dayglow decreases observed with AIRS and resulting from the hypothesized water-vapor cloud (~ 50 km diameter) should be multi-pixel events.

Frank *et al* [reply to Chubb, 1986] reported many cases of a hole that was observed in adjacent scan lines. Observation of a hole in an adjacent scan line for the AIRS sensor would depend upon many variables, such as the motions of both the satellite and the water-vapor cloud, but it should occur in slightly less than half of all observed holes. This is illustrated in Figure 2, where a lateral velocity of 11 km/sec is assumed [Frank *et al* (reply to Chubb), 1986]. The rate at which a hole should be observed in an adjacent scan line for AIRS is a function of the higher sweep rate (three sec for Polar BEAR, as opposed to six sec for DE-1).

The observing characteristics in a search for intensity decreases with the AIRS instrument are favorable. If the mini-comet hypothesis is correct, then the water-vapor cloud should be moving downward with a velocity of ~15 km/sec. The Polar BEAR satellite was approximately 700 km above the main ionospheric region emitting VUV dayglow. Thus the total time that the hole is at an altitude below the satellite and above the dayglow region was ~45 seconds. Frank *et al* [1986] estimated the comet influx to be on the order of 20/minute, which translates to 0.33 comets per second. Thus, at any time, there should be about 14.8 water-vapor

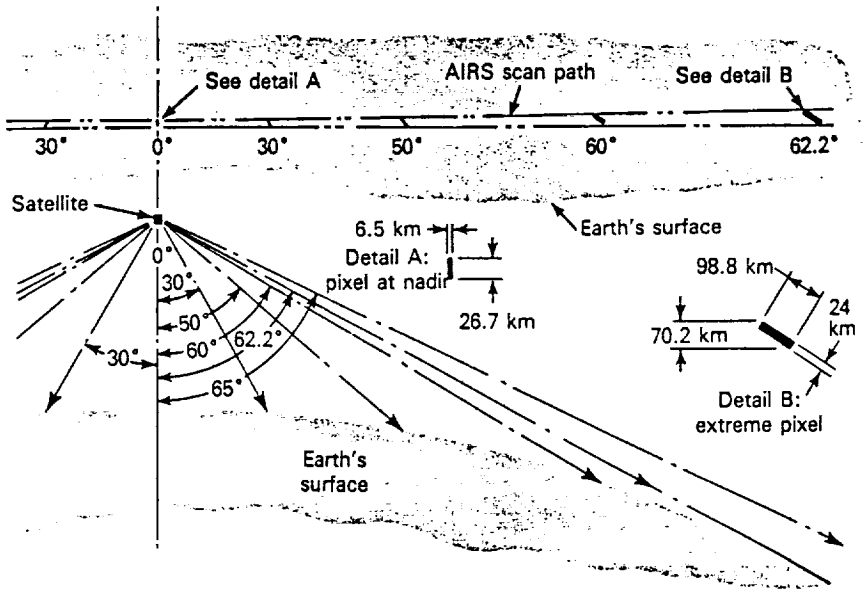

Figure 1. AIRS pixel-footprint projection as a function of image scan-path angle (Schenkel and Ogorzalek, 1987).

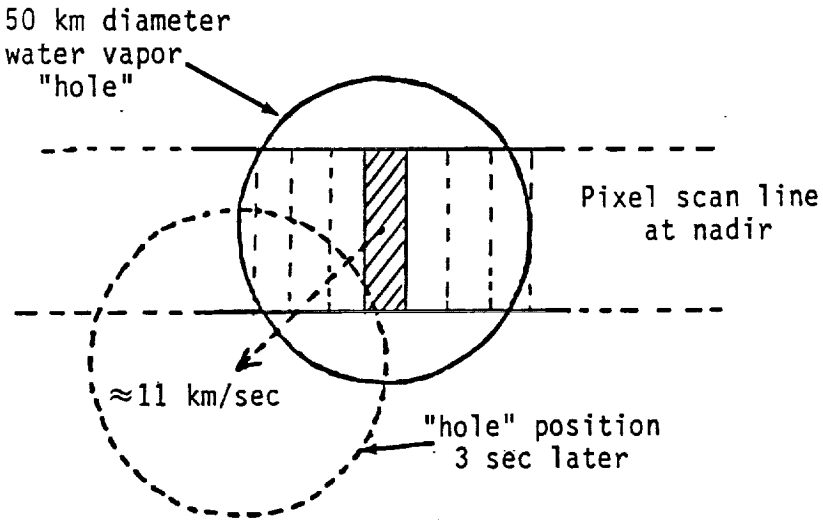

Figure 2. Polar BEAR AIRS sensor pixel footprint at nadir as compared to postulated atmospheric hole diameter. In this scan line about seven pixels would be obscured. The dotted hole shows position of the hole three seconds later, assuming a lateral velocity of 11 km/sec. The hole should obscure pixels in the adjacent scan line about half the time.

clouds (45 sec x 0.33 comets/sec) in the spherical shell volume bounded by the satellite altitude and the dayglow region altitude. For each pass of the Polar BEAR satellite, the AIRS imager swept out a triangular region with a height of ~700 km, a base of ~2400 km, and a length of ~4000 km. (See Figure 3.) Thus the total number of holes observed with each pass should be the ratio of the volume the imager swept out (V_i) divided by the spherical shell volume (V_s) multiplied by the average number of water-vapor clouds in the spherical shell:

$$\#\ \text{holes per image} \sim \frac{V_i}{V_s} \times 14.8\ \text{holes}$$

$$\sim \frac{1/2 \times 700\ \text{km} \times 2400\ \text{km} \times 4000\ \text{km}}{4/3\ \pi \times [(7375\ \text{km})^3 - (6675\ \text{km})^3]} \times 14.8\ \text{holes}$$

$$\sim 0.11\ \text{holes per image.}$$

Although these numbers are estimates, the overall expectation is that over 10% of the full dayglow image passes should show a set of pixel decreases associated with an atmospheric hole. Several other methods of estimating the number of holes per image have been used, and they result in similar values. It should be noted that this estimate is in rough agreement with the number observed by DE-1. Frank *et al* [1986] observed three to five holes per dayglow image. If the typical DE-1 image shows a dayglow region corresponding to 25% of the earth's surface, and the typical Polar BEAR image shows a dayglow surface of ~2% of the earth's surface, this would imply 0.24 to 0.4 holes per Polar BEAR image. The more accurate estimate, calculated above, is somewhat lower than this value because the water-vapor clouds will be observed only when they are below the Polar BEAR altitude and in the field of view of the AIRS sensor.

The AIRS instrument data set should be capable of detecting atmospheric holes if the mini-comet hypothesis suggested by Frank *et al* [1986] is correct. Of more importance is that the satellite, at a much lower altitude, should have a different signature from that of DE-1 images. In addition, since the satellite was at a much lower altitude and the scan lines repeated at twice the rate of DE-1, any holes detected should be multi-pixel events, with a high probability of detection on an adjacent scan line. This would yield much more detail about the characteristics of the holes.

III. DATA-ANALYSIS PROCEDURE

The Polar BEAR data set (a copy of which is located at Northwest Research Associates [NWRA]) is stored on approximately 900 9-track magnetic tapes. Fortunately for this study, NWRA proceeded with the task of archiving the entire useful Polar BEAR imager database into a magneto-optical disk format for Phillips Laboratory (PL) of Air Force Systems Command during a previous contract. Although this magneto-optical disk set was sent on to PL, a copy of this data set (comprising over 5500 image files) was also stored on five 8mm magnetic-tape cartridges (2.2 Gbytes capacity per tape) for use at NWRA. This magnetic-tape cartridge drive

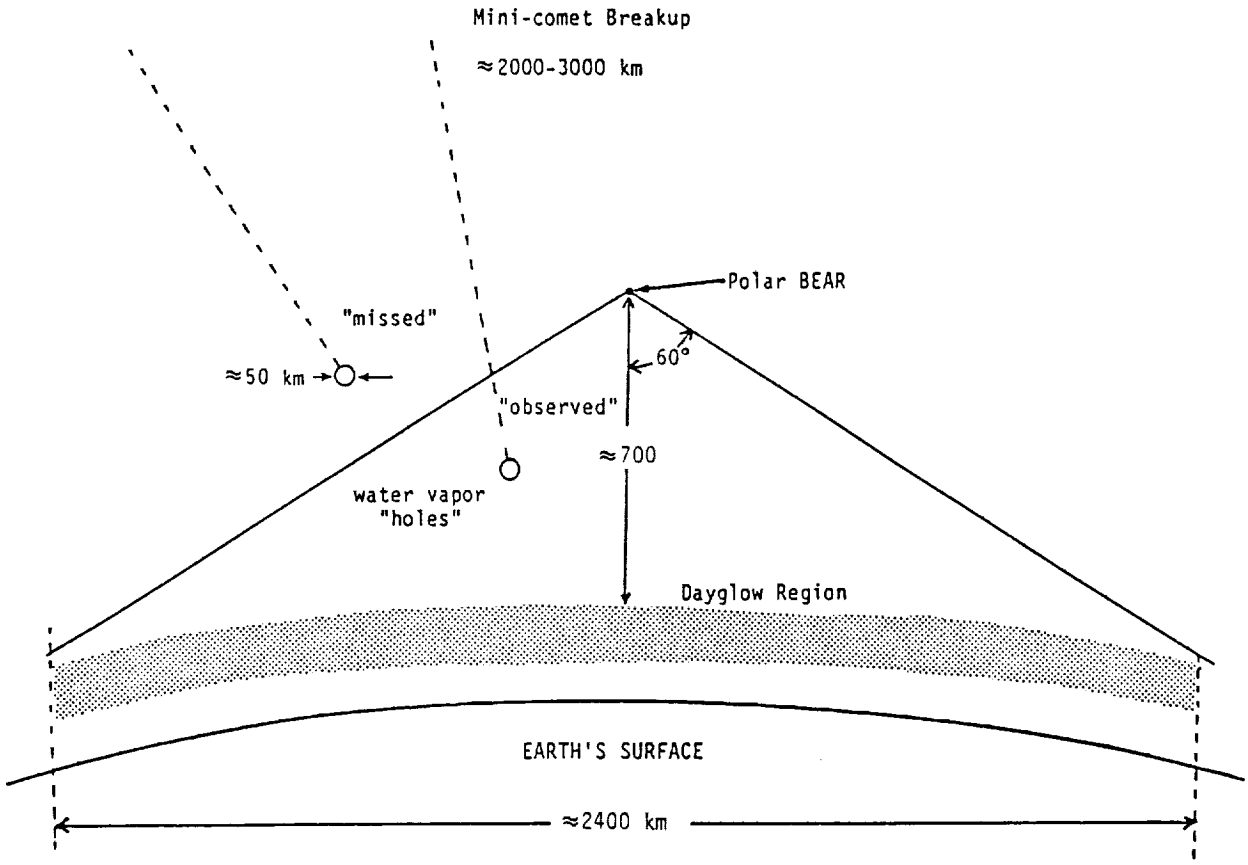

Figure 3. Angular view from Polar BEAR satellite swept out a triangular volume (satellite motion is perpendicular to page). Holes within the angular scan range should be observed against the dayglow region background.

is attached to the Sun-4/280S computer at NWRA. A Silicon Graphics Personal Iris is networked to the Sun-4, and thus the data set could be accessed by either machine.

The first procedure was to reduce the image data set to a size that would fit on one 8mm magnetic-tape cartridge, so that the processing could be run in a low-priority "batch" mode at night. The data of primary interest were taken with the VUV channel in the 130.4-nm mode, as this had the greatest intensity in the form of dayglow. After preliminary examination of the data, it was decided to include data taken with the VUV channel in the 135.6-nm mode. There were actually more data for the 135.6-nm mode than the 130.4-nm mode, even though the 135.6-nm data had generally lower intensity levels.

A program was designed to act as a filter to read in the individual image files from the large database, determine if the data contained either 130.4 nm or 135.6 nm data, and then examine the maximum sun-sensor angle (stored along with the image in the file). The sun-sensor angle is the angle of the sun's elevation above the horizon (the plane defined by 90 degrees from the satellite nadir). If this angle was greater than 25 degrees for 130.4 nm data (40 degrees for 135.6 nm data) the image data file was moved to disk. This procedure of eliminating image data with low sun-sensor angle insured that the images processed should have some dayglow data in the image field.

After the filter program was developed, but before use with the large data set, a copy of the program was extensively modified to run on the Silicon Graphics Iris and use the Graphics Library calls to place a color-coded AIRS image onto the Iris screen. An example of the output of this program is shown in Figure 4a. The top portion of this figure shows the basic screen graphic plot with four sub-panels for each of the four detectors on the AIRS instrument. The color coding is for the entire count range (0 - 8032) in the "packed" (semi-logarithmic) form, with dark blue for low and bright red for highest counts. The upper two detectors are set for the visible range and thus are typically saturated near the terminator region, causing the pixel counter to cycle through its range (the curving diagonal color bands). The lower left sub-panel is for the VUV detector 1, which ceased functioning early in the mission and thus typically shows dark blue, indicating no pixel counts. The lower right sub-panel shows detector 2, which is set at 130.4 nm. Under menu control, any sub-panel could be expanded as shown in Figure 4b. This expansion of the 130.4 nm sub-panel above shows several typical features. A strong auroral band is shown across the center of the image (showing a downward turning near the edges as distortion when viewing near the horizon). The dayglow region in this figure is only the top portion of the image and extended somewhat further down on the left portion of the image than the right (similar to the terminator seen in the visible light detectors in Figure 4a). At the side of the image(s) is a portion of the screen devoted to displaying the individual pixel counts for a 10x10 pixel region pointed to (under mouse control) by the red arrow seen in the image panel. This visual program permitted individual examination of any potential scan-line depletion candidates suggested in the main study.

Information concerning the sun-sensor angle was placed in another window while using the graphics program. This program was used to determine the minimum value of sun-sensor

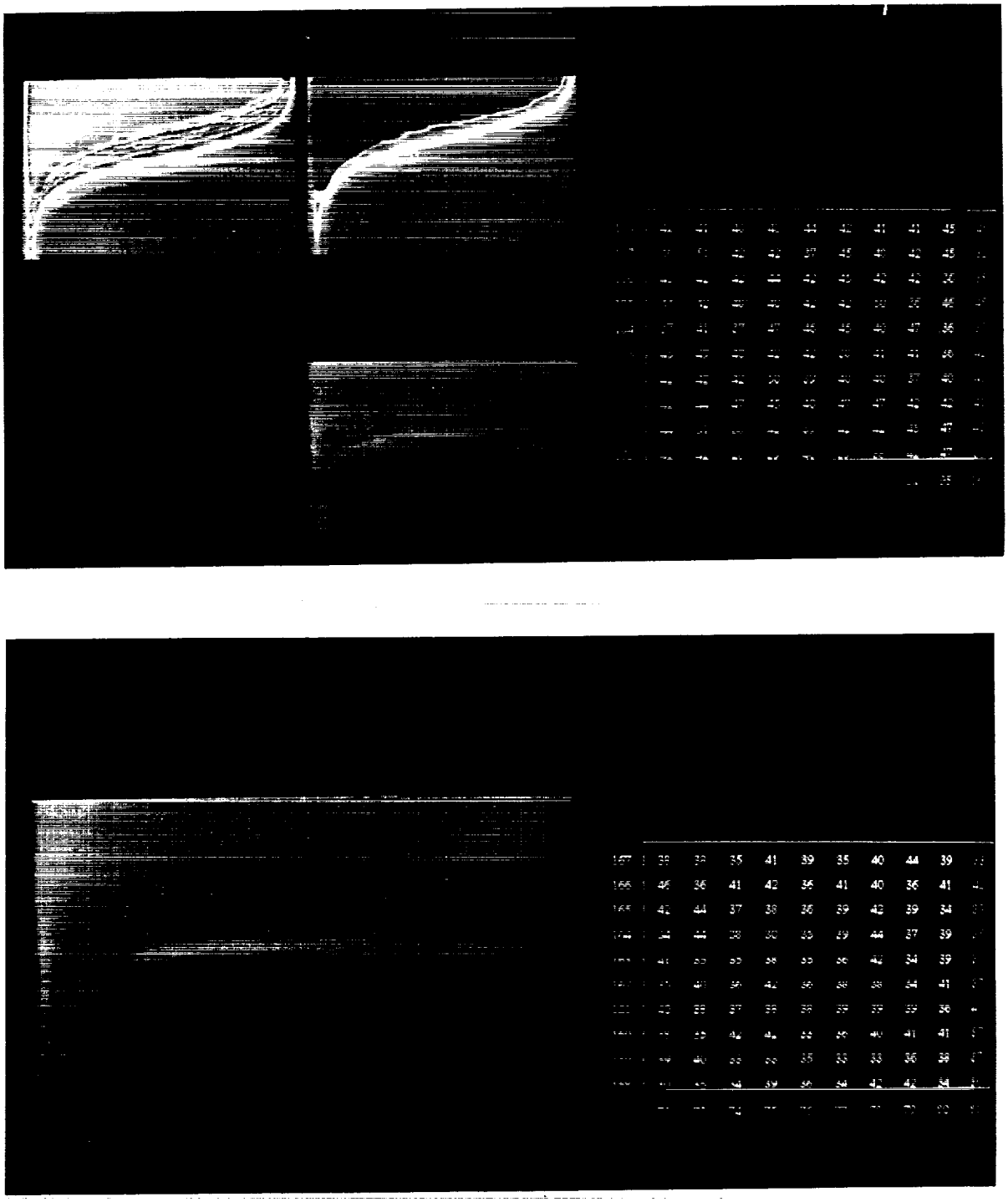

Figure 4. Example image showing display from Silicon Graphics IRIS for December 18, 1986 at 18:53 UT. The top portion (a) shows data from all 4 detectors and the pixel counts for the group near where the red arrow is placed. The bottom portion (b) shows data from just Detector 2 (the 1304-nm data) and the pixel counts near where the red arrow is placed. Note that only the portion above the auroral band in (b) would constitute dayglow used in this study.

angle that would have useful dayglow. The minimum sun-sensor angle value for 135.6 nm was set higher than that of 130.4 nm, due to its lower intensity.

The next procedure was to extract data files from one of the five 8mm tapes and place these files onto disk, then run the filter program to select files that should have some dayglow data. This process continued until the Sun-4's disk was nearly full, then the accumulated image files would be placed in groups of 50 onto another 8 mm tape in standard Unix tar format. This procedure was continued until the data from all five 8mm tapes were processed and reduced to a single 8mm "master" tape. As a result of this procedure, the entire data set utilized for this study was placed on a single tape cartridge that contained 1538 image files (each file averaged ~ 400 Kbytes). These files were arranged in groups of 50 files, which was an appropriate amount given our system's working-disk capacity. Of these image files, 650 were 130.4 nm data and 889 were 135.6 nm data. Unfortunately, at this point in the procedure, we had a failure of a "master" tar tape, and the process was repeated to produce two copies of the "master" tar tape. Thus, a backup "master" was made, which could be used without going through the entire data-processing procedure again. With the data of interest stored on one 8mm tape, a version of the filter program was modified to identify potential hole candidates for further examination.

Since the goal of this study was to seek out pixel-string intensity reductions produced by water-vapor clouds as hypothesized in Frank *et al* [1986], we will list some of the expected properties. Frank *et al* [1986] described the water-vapor clouds as being approximately 50 km in diameter, producing an intensity reduction of greater than 4.3σ in an image pixel compared to the surrounding six pixels (three on each side). Assuming Poisson statistics hold for n (intensity counts in each pixel), $\sigma = \sqrt{n}$. Given the typical pixel intensity in the DE-1 image of ~ 50, this required that the reduced-intensity image pixel had an intensity in the range of 0% to 40% of the surrounding six pixels. (Frank *et al* [1986] indicated typical response rates of ~ 10 counts/pixel in a hole, with typical count rates of ~50 counts/pixel in dayglow.) Since the water-vapor cloud subtends an angle only slightly smaller than that of the pixel as observed from typical DE-1 altitudes, the water-vapor cloud should be essentially opaque to light in the 130.4 nm spectral line [Watanabe and Zelikoff, 1953]. As is illustrated in Figure 3, the water-vapor cloud can range from about 3000 km from the AIRS instrument on Polar BEAR (off-nadir viewing) to being directly under it. However, the distance typically should range from 2000 km to 300 km. Given a 50-km diameter water-vapor cloud, the angular width will range from 1.43 degrees to about 9.5 degrees. Since the pixel width on AIRS is 0.4 degrees, such a hypothesized cloud should cause an intensity decrease in a string of from 3 to 23 pixels. Although there may be clouds of smaller size, these would not have been observable from the typical DE-1 altitude and therefore would not be included in the statistics described in Frank *et al* [1986]. The search characteristics were for a string of pixels in a single scan line to be of significantly decreased-intensity levels as compared to surrounding pixels. The string of decreased-intensity pixels would be from 3 to 23 pixels in length. If such a string of decreased-intensity pixels were found, then adjacent scan line(s) may include a similar string of decreased-intensity pixels.

The data-analysis procedure was to modify the basic program to seek candidates for a dayglow intensity decrease of the type described in the preceding paragraph. This program used a set of modifiable parameters to search the entire data set and list possible candidates to be

directly examined using the image-viewing program. It was believed at the start of this study that selection criteria could be found that would eliminate false alarms due to intensity variations of auroral bands typically observed in most of the images. (See Figure 4b.) However, after some preliminary work and many thousands of false alarms, it was found necessary to determine visually the acceptable scan-line numbers (portions of the images with no auroral bands). This information was used so that the program would ignore portions of each image that had an auroral band. This entailed a lengthy visual search through all images. Although this search was to find and build a list to eliminate aurora in the images, it also provided a chance to search the database visually. No clear case of decreased-intensity pixels was found during this visual search.

The data set contained relatively few cases where the entire pass was over a dayglow region. The northern hemisphere has strongly daylit conditions during the summer period. The data obtained by AIRS during this period were limited for two reasons. Difficulties arose due to mechanical problems with the satellite attitude-control system [Hunt and Williams, 1987], and periods occurred in which the scanning mirror stuck [Richard Eastes, private communication]. Thus, a great portion of the data-image set included a terminator region with a continuously increasing or decreasing intensity in the dayglow. Figure 4b shows an example of such a region. The use of images with significant terminator data often had average pixel values too low to be effective for this type of study. If, for example, the pixel-counts statistics averaged lower than 25, a value of 0 for a given pixel would be less than 5σ below the average. In addition, a significant portion of the data was at 135.6 nm, which had a significantly reduced intensity compared to 130.4 nm. Since all intensity depletions must be multi-pixel events for this search, it was common to add M pixels together at once, forming a summed pixel. This sacrificed spatial resolution for greater intensity in the counts. Three common M values used for this purpose were 5, 10, and 15. These were chosen since a summed-pixel decrease would show up for at least one of these M values for a string of pixel intensity decreases for our estimated string of 3 to 23 pixels.

A parameter that was varied for our search program was called NGRP. This was the total number of (summed) pixels (exclusive of the one being tested) being averaged together to determine the average intensity. Frank *et al* [1986], in their single pixel groupings, used six (three on each side of the pixel being tested). While the value of six was also used extensively in our study to compare our results more closely to Frank *et al* [1986], this limited the number of summed pixels in the scan line. For example, using the case of M = 10 (pixels being grouped 10 at a time) and NGRP = 6, a total of 70 pixels along the scan line are involved in each test (the 10 in the super pixel being examined, as well as 30 on each side of it). The value of NGRP = 4 was used as well. Although the grouping of pixels by groups of M was used, the movement of the test region along a scan line proceeded by increments of one pixel. This way an intensity reduction of a string of M/2 pixels would not be undetected by being split between two summed-pixel groups.

After some preliminary work, two other parameters were set at ST_LN = 20 and END_LN = 305 (used for all data shown in this report). These parameters were the start and stop pixel numbers in the scan line to be used for the data search. These were not left at 0 and

325 because there was typically strong limb brightening as the mirror scan pointed near the limb of the image. (See left side of the image shown in Figure 4b.) The gradual increase in pixel intensity from the center of the image to the limb could be adjusted for in the program criteria, but the extreme intensity gradient near the edge produced false alarms in large magnitudes from this extremely common event. It was easy to adjust the limits on the scan line to prevent these, but there were still some cases that could not be handled this way due to the attitude-control problem mentioned earlier. During the satellite-attitude oscillations, the limb brightening would swing rather strongly and sinusoidally in the image rather than effecting a vertical intensity enhancement near the extreme edges of the image. A few of these images produced false alarms that were eliminated during the final candidate inspection.

There was an additional problem. On occasion, there were a small number of "red" pixels scattered throughout the upper portion of many of the images. Red indicated a very high count rate for the data being observed. These pixels were attributed to occasional radiation-belt particles randomizing the accumulating counter [Richard Eastes, private communication]. Since the data were stored most of the time in packed form on the satellite, if the bits changed by radiation were essentially random, the "false" pixels would be scattered in a semi-logarithmic manner. Thus, most of the "false" pixels would be radically higher than their nearest neighbors for typical dayglow intensities. However, some pixels will be a false low value. For this reason, single-pixel intensity decreases must be regarded as radiation-belt effects or water-vapor clouds so small as to be undetectable from DE-1's typical orbit (*i. e.*, not included in the Frank *et al* [1986] statistics).

Once parameters M and NGRP were set, all of the image data were examined for potential summed-pixel intensity reductions corresponding to a string of pixels being statistically significantly darkened compared to the surrounding running mean. A number of pixel situations were not included in the statistical base after determining that the pixel set met certain conditions. This was to avoid excessive false candidates. These situations included:

1. If the summed-pixel average preceding the summed pixel being tested differed from the summed-pixel average following the test summed pixel by a factor of two, the intensity gradient was assumed to be too large for the depletion study. This often occurred near the border of the viewing field, where the edge enhancements occurred.

2. If any single summed pixel in the group was greater than or equal to four times the average value for the NGRP of summed pixels, it was clearly dominating the average, and the case was pathological.

3. If the summed-pixel average for the total NGRP of summed pixels was less than 36, this would mean that the maximum number of σ away from the average for any intensity depression would be -6 (*i. e.*, the intensity is too low for good statistics).

4. If any pixel in the set being examined was greater than twice the sum of both the preceding and the following pixels, this typically was a case of a "red" pixel found to be associated with a radiation-triggered counter event.

Two files were output from each of the search results. One contained the statistics of each image examined in which the data were binned by the R (the number of standard deviations from the running mean of surrounding pixels, measured in σ) values that each summed pixel varied from the surrounding averages. In a manner similar to Frank *et al* [1986], we chose a bin size of 0.2σ. The second file contained all possible candidates for a pixel-intensity reduction as hypothesized by the small-comet hypothesis. Each candidate case was listed by scan-line number and pixel number (center of summed pixel) along the scan line, as well as the parameter, M, for the case, the actual summed-pixel values (typically either five or seven values for cases of NGRP equal to four or six). Also listed was the R value.

IV. RESULTS

The results of this study are interpreted in relation to the original Frank *et al* [1986] study. Shown in Figure 5 is a copy of Figure 1 taken from Frank *et al* [1986]. This figure shows the statistical results of the binned data from a set of dayglow images taken from DE-1. In this figure a total of 1.3×10^6 samples (pixels) are used to determine the counting statistics of the pixel decreases. The distribution is a function of the number of standard deviations, R, from a running mean of six samples, where the running mean is taken from the three consecutive samples each prior to and following the sample pixel.

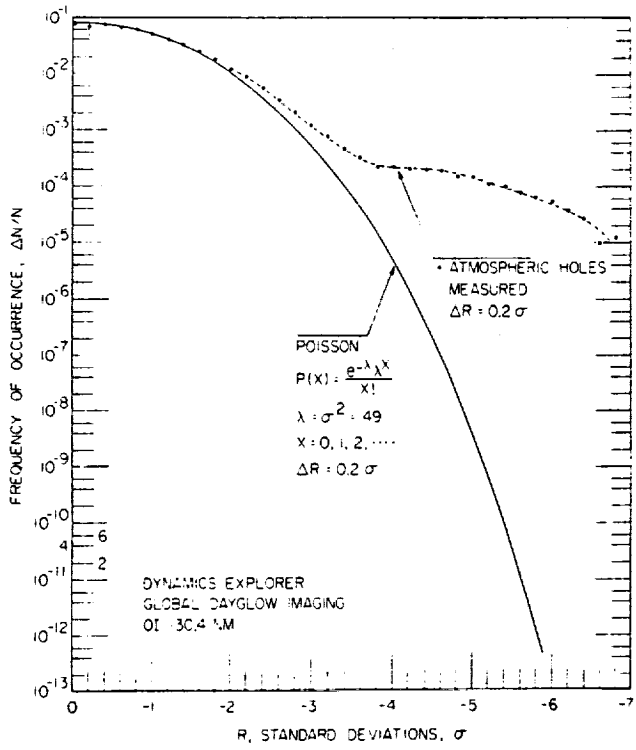

Figure 5. Comparison of the distribution of approximately 1.3×10^6 samples (pixels) of dayglow intensities at OI 130.4 nm with the expectations for a Piosson distribution with mean rate of 49 counts/pixel. An atmospheric hole is identified with any pixel for which $R \leq -4.3\ \sigma$. Taken from Frank *et al* [1986].

The statistical results of this study (Figures 6 to 9) are displayed in a similar manner to that of Frank *et al* [1986] to facilitate comparison. Note in particular that the bottom axis showing the standard deviation of the binned AIRS data has reversed sign, such that the excess tail on the right of the distribution corresponds to large negative (decreased intensity) R value. There is a slight difference in scale, and the binned data in this study show the positive values of R as well as the negative ones. Some examples of the DE-1 data set showing the positive values of R were shown in Frank *et al* [1987b]. A sample Poisson distribution is not shown for our cases. The DE-1 image data had relatively uniform intensity distribution over the scanned area. The AIRS data used for this study were often near a dayglow terminator, with a varying intensity. Despite the varying intensity, the figures show a clearly Poisson-like distribution about the local average intensity at zero.

The first set of data shown in Figure 6 used the parameter, NGRP = 6. This means that the summed-pixel value being tested was compared to the average of the preceding three and the following three summed-pixel values. Figures 6a - 6f shows the binned data for the cases of the summed-pixel value of M = 15, 10, 5, 3, 2, and 1 for 130.4 nm data. For the M = 15, 10, and 5 cases, the total sum (N) of the pixel groups was on the order of 5×10^6. It is for one (or more) of these values of M that a string of 3 to 22 decreased-intensity pixels will produce a large negative R value. It is in these first three panels where we expect to see intensity reductions of a similar statistical nature to the Frank *et al* [1986] study. It is clear from Figures 6a - 6c that the increase in the tail of the distribution curve for R values less than -4.3, observed in the Frank *et al* [1986] study, does not show up. There is a hint of increase for R values lower than -5 in Figure 6b, and a clear increase in Figure 6c. These will be discussed later.

Figures 7a - 7e shows similar binning of the data for 135.6 nm. There is a clear increase in the tail for R values lower than about -5 for Figures 7a and 7b. The sum (N) of data points for the M = 5, 3, and 2 cases rapidly decreases. This is because the 135.6 nm data have lower intensity values than the 130.4 nm data (even though there are more data). Summing fewer than five pixels reduces the intensity counts to a point that Poisson statistics cannot have large negative R values. In the 135.6 data in Figures 7a and 7b, there seems to be a clear and small increase for R values less than -5. Figure 7c shows some missing points (no events in bin) for R values less than -5, and clearly the low intensity values of this data set are affecting the distribution tail (the sum N value is only 3.173×10^5). For the lower values of M in Figures 7d and 7e the sum (N) is clearly too low for useful statistics.

To verify the trends observed in these figures, Figures 8a - 8f shows the 130.4 nm data binned again using a value of NGRP = 4 (a shorter running average). For these binned data, only the preceding two and following two summed-pixel values were used in the running average. The results of this new grouping for the running average show essentially the same features as in Figures 6a - 6f, even though the sum (N) was slightly increased. Figures 9a - 9e shows the 135.6 nm binned data also using the value of NGRP = 4 and the same features as Figures 7a - 7e.

In addition to the file containing the statistically binned data, a file for each run was produced which contained the summed-pixel counts for any case where the R value was less than a set value (usually chosen to be -5.0). This file also contained any set where the summed

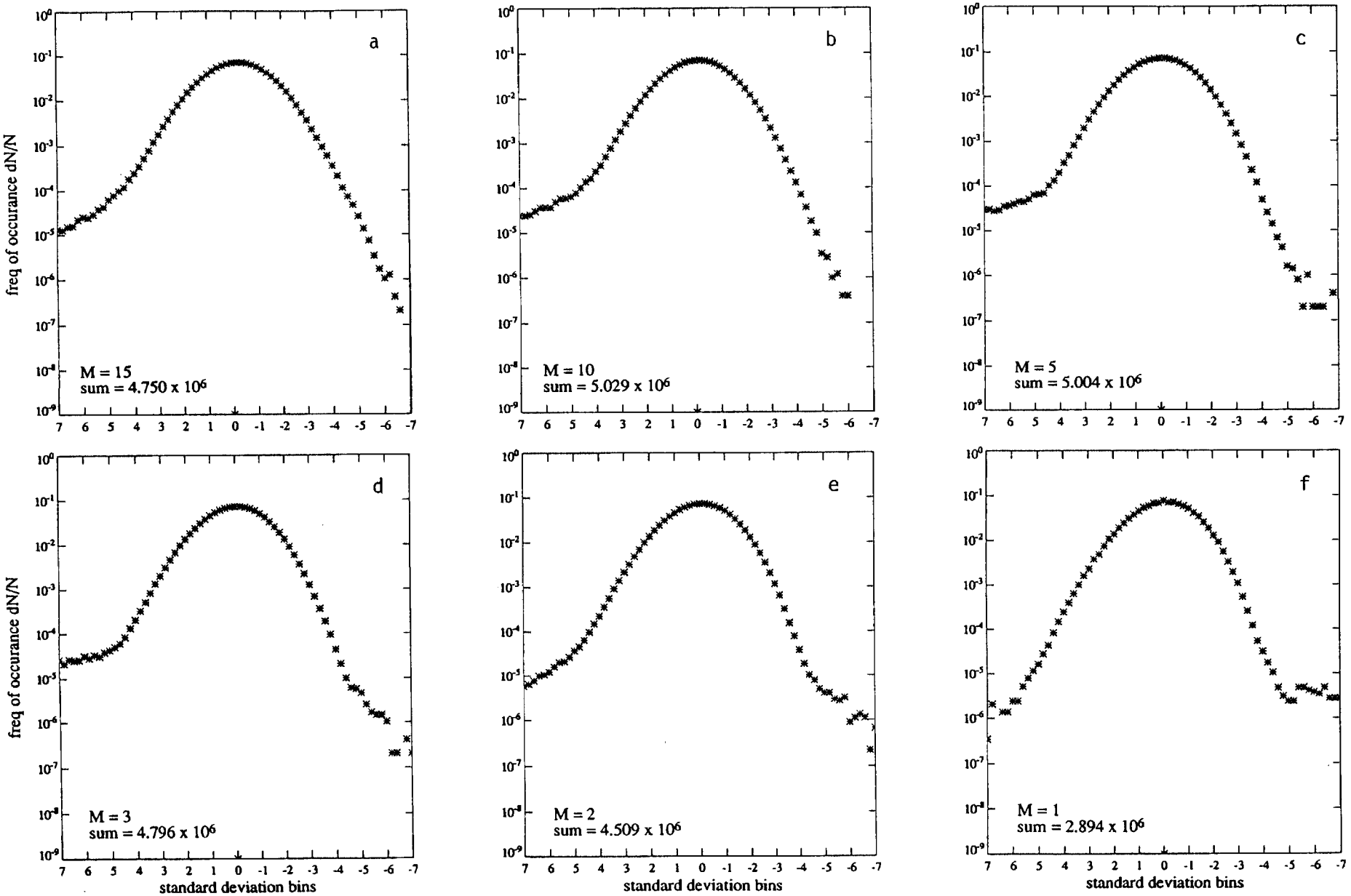

Figure 6. The AIRS 130.4 nm data binned by the number of standard deviations (R) away from the running average. The bin size was 0.2σ. NGRP = 6 (the number of pixel groups forming the running average). In each case the pixels were grouped or summed by the value, M. Both M and the total sum (N) of pixel groups binned are shown in the lower left hand corner of 6a - 6f.

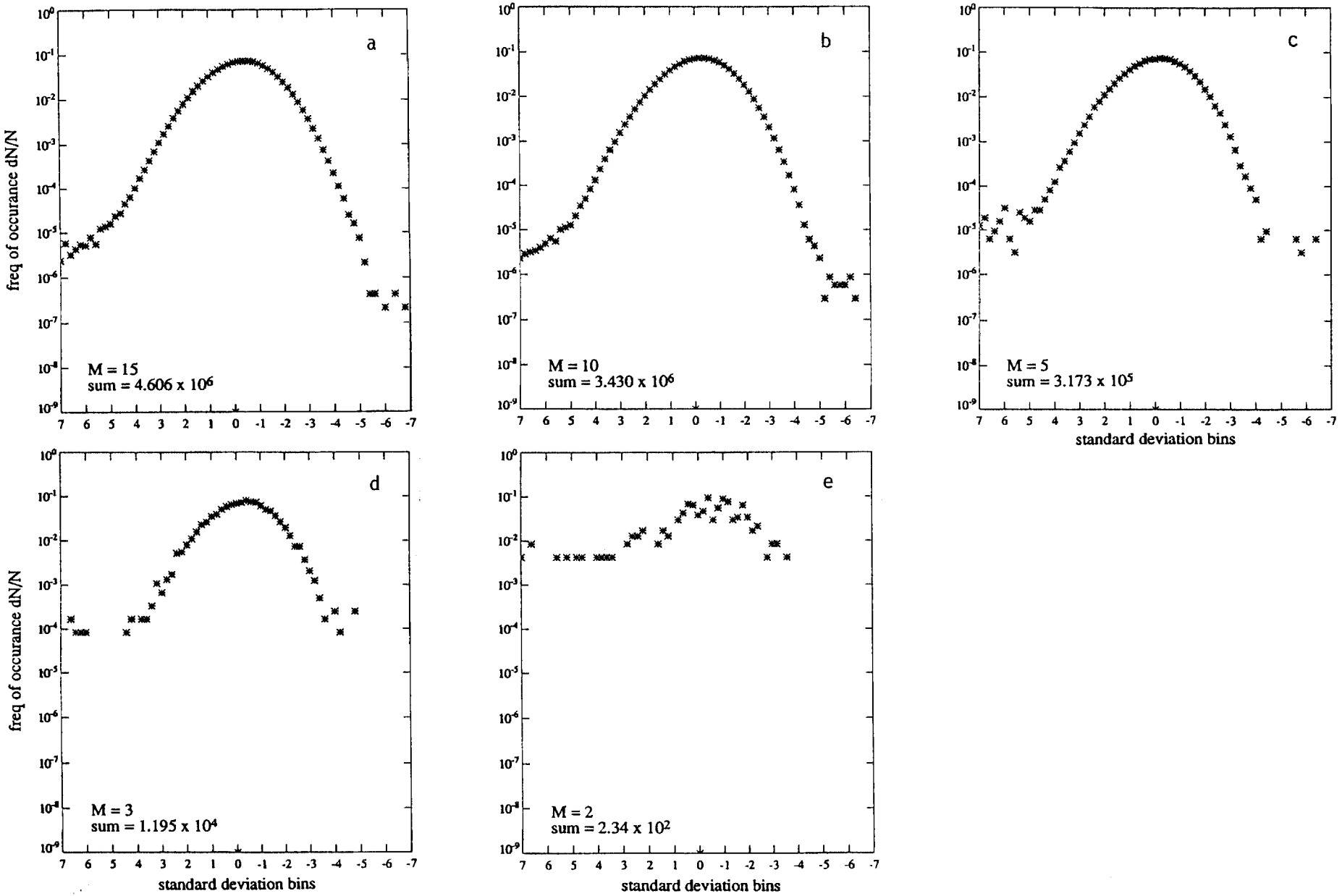

Figure 7. The AIRS 135.6 nm data binned by the number of standard deviations (R) away from the running average. The bin size was 0.2σ. NGRP = 6 (the number of pixel groups forming the running average). In each case the pixels were grouped or summed by the value, M. Both M and the total sum (N) of pixel groups binned are shown in the lower left hand corner of 7a - 7e.

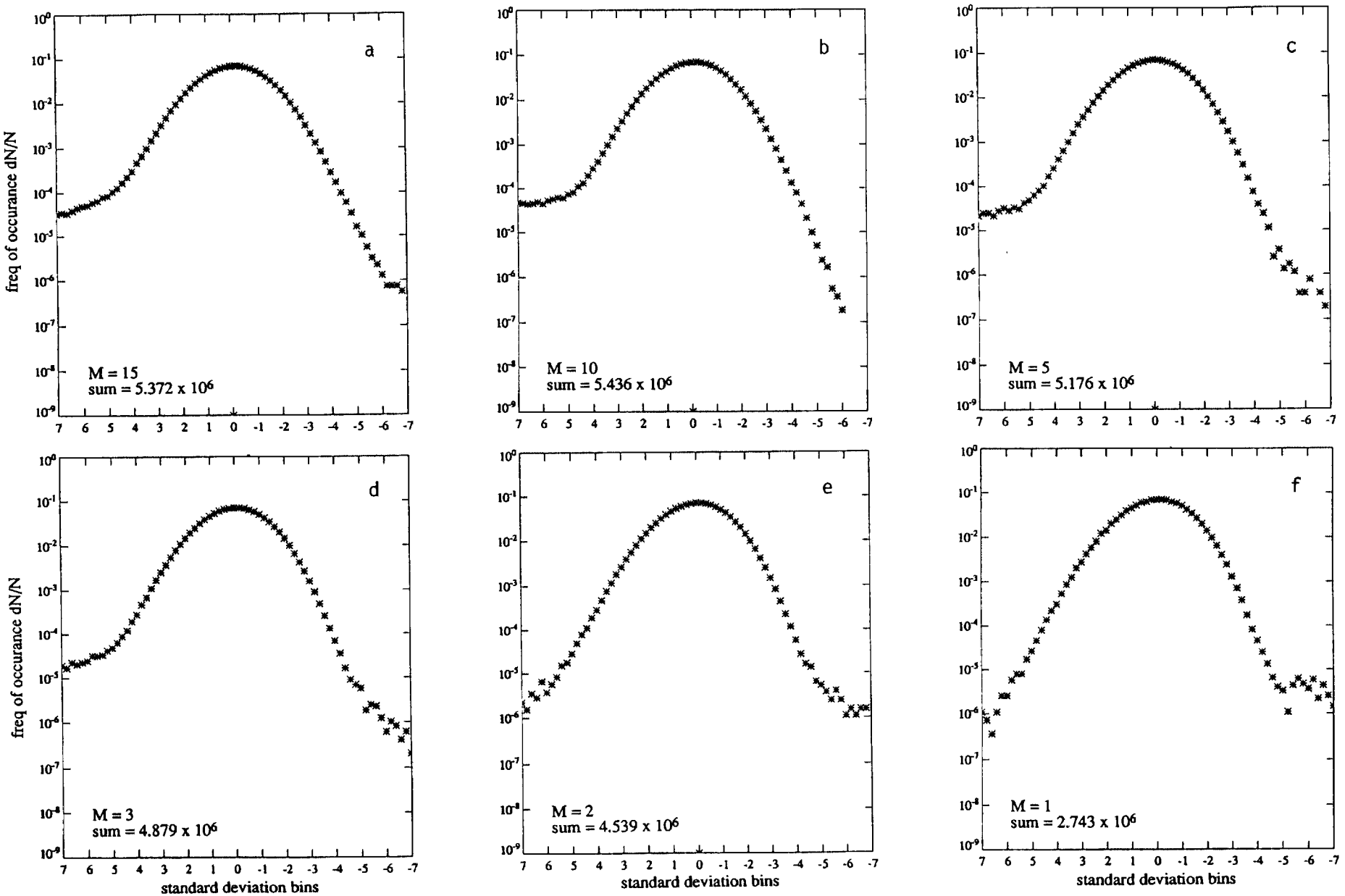

Figure 8. The AIRS 130.4 nm data binned by the number of standard deviations (R) away from the running average. The bin size was 0.2σ. NGRP = 4 (the number of pixel groups forming the running average). In each case the pixels were grouped or summed by the value, M. Both M and the total sum (N) of pixel groups binned are shown in the lower left hand corner of 8a - 8f.

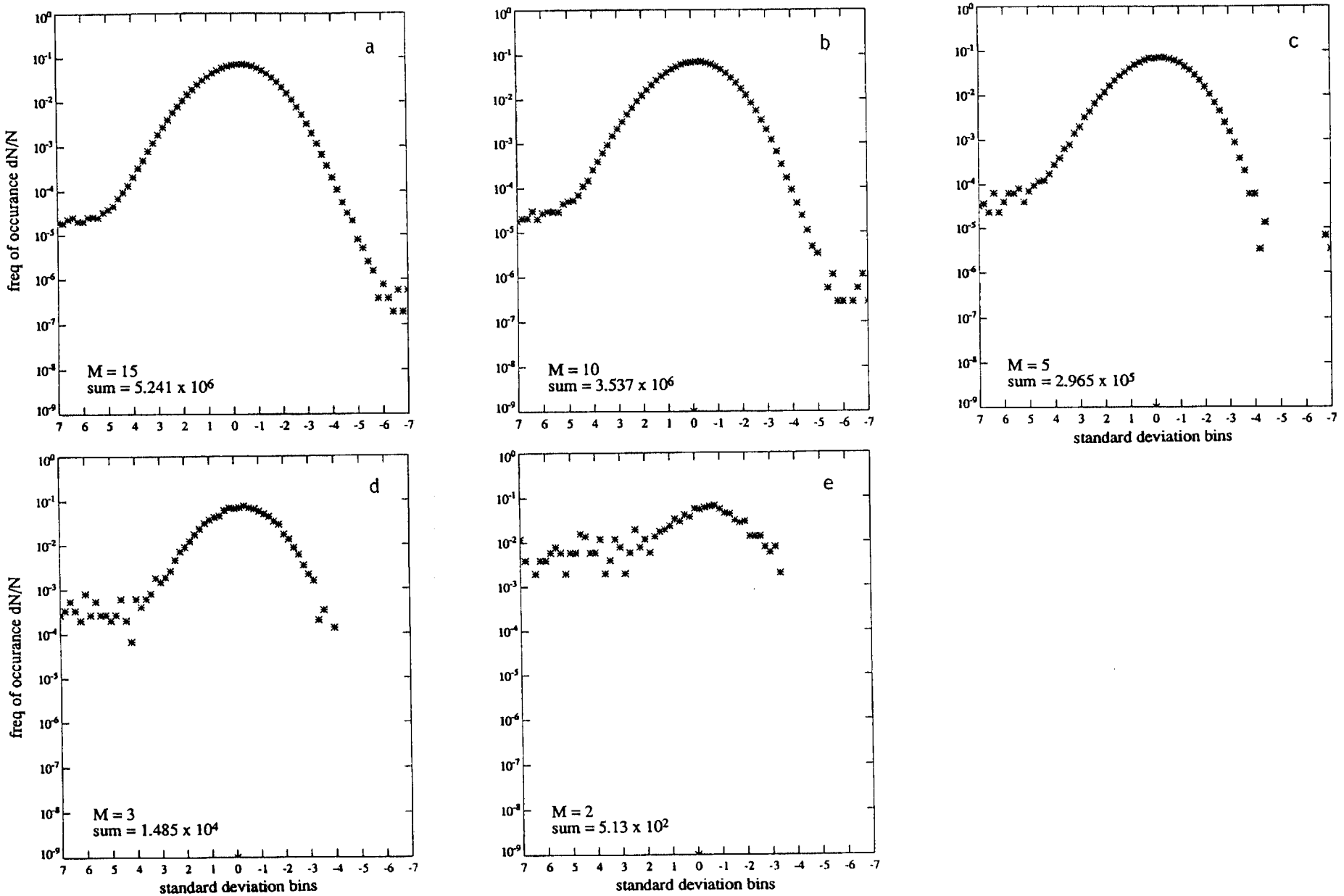

Figure 9. The AIRS 135.6 nm data binned by the number of standard deviations (R) away from the running average. The bin size was 0.2σ. NGRP = 4 (the number of pixel groups forming the running average). In each case the pixels were grouped or summed by the value M. Both M and the total sum (N) of pixel groups binned are shown in the lower left hand corner of 9a - 9e.

pixel in question was less than 50% of the intensity of the running average. Some cases could be eliminated as potential "holes" candidates due to some obvious problem with the data (*e.g.*, one summed pixel in the running average being much larger and dominating the others). All other cases were examined individually using the image- and pixel-scanning program for the Silicon Graphics Iris. A vast majority of these cases were found to be due to one pixel being extremely low in value in the summed pixel being examined. These individual pixels are believed to be the low-intensity counterparts to the radiation-induced bright pixels described in the previous section.

For the case where the summed-pixel counts in question were less than 50% of the intensity for the running average, using groupings of M = 5, 10, and 15, it was found that these were typically cases of low intensity (36 to 75 counts). They were shown typically to have R values of -3 to -5 and thus to be part of the standard Poisson distribution. Two exceptions (both found in the 135.6 nm data) will be presented.

The two best candidates from the 130.4 nm data are shown in color in Figures 10a and 10b. Figure 10a is image file pb306104, which started March 12, 1989, at 16:11 UT. Figure 10b is image file pb184836, which started December 24, 1986, at 21:58 UT. Both images have a large black circle to focus attention on the portion of the scan line of interest. The figures are color coded with pixel values of 0 being dark blue, and pixel values of 60 or above being red. The color range was linear for pixel values from 1 to 60.

For these cases the scan-line data are plotted out in Figures 11a and 11b, showing the pixel counts versus pixel position along the scan line with an arrow indicating the intensity reduction. Figures 12a and 12b show the counts of the pixel field where the pixels comprising the event are indicated. The top two lines of Table 1 show the summed pixel values associated with these two events. Note that the total intensity in both of these cases was only 76% and 80% of the running average rather than the value of ~20% reported by Frank *et al* [1986]. Table 1 shows that the events had R values of -5.20σ and -5.23σ. From Figures 6a, 6b, 8a, and 8b, we see that for an R value of -5.2σ the curves are still quite smooth, with values of $\sim 10^{-6}$, and show no unexpected deviations from the approximately Poisson distribution shown.

In a similar manner, Figures 13a and 13b show the color images for the two best candidates in the 135.6 data. Figure 13a is image file pb225134, which started February 20, 1987, at 08:44 UT. Figure 13b is image file pb223918, which started January 30, 1987, at 10:32 UT. Similarly, Figures 14a and 14b show the pixel counts versus pixel position along the scan line, and Figures 15a and 15b show the counts of the pixel field for the two 135.6-nm best candidates. The last two lines of Table 1 present the summed-pixel values for each of these cases as well as the R value for each of these four cases. Here, the R values are -5.32σ and -5.18σ. Although the count rates are lower than the 130.4 nm cases, the total intensity is only 39% and 46% of the running average. As seen in Figures 7a, 7b, 9a, and 9b, it is for R values of between -5 and -6 that there is some indication of an increase in the distribution greater than that accounted for by the Poisson distribution.

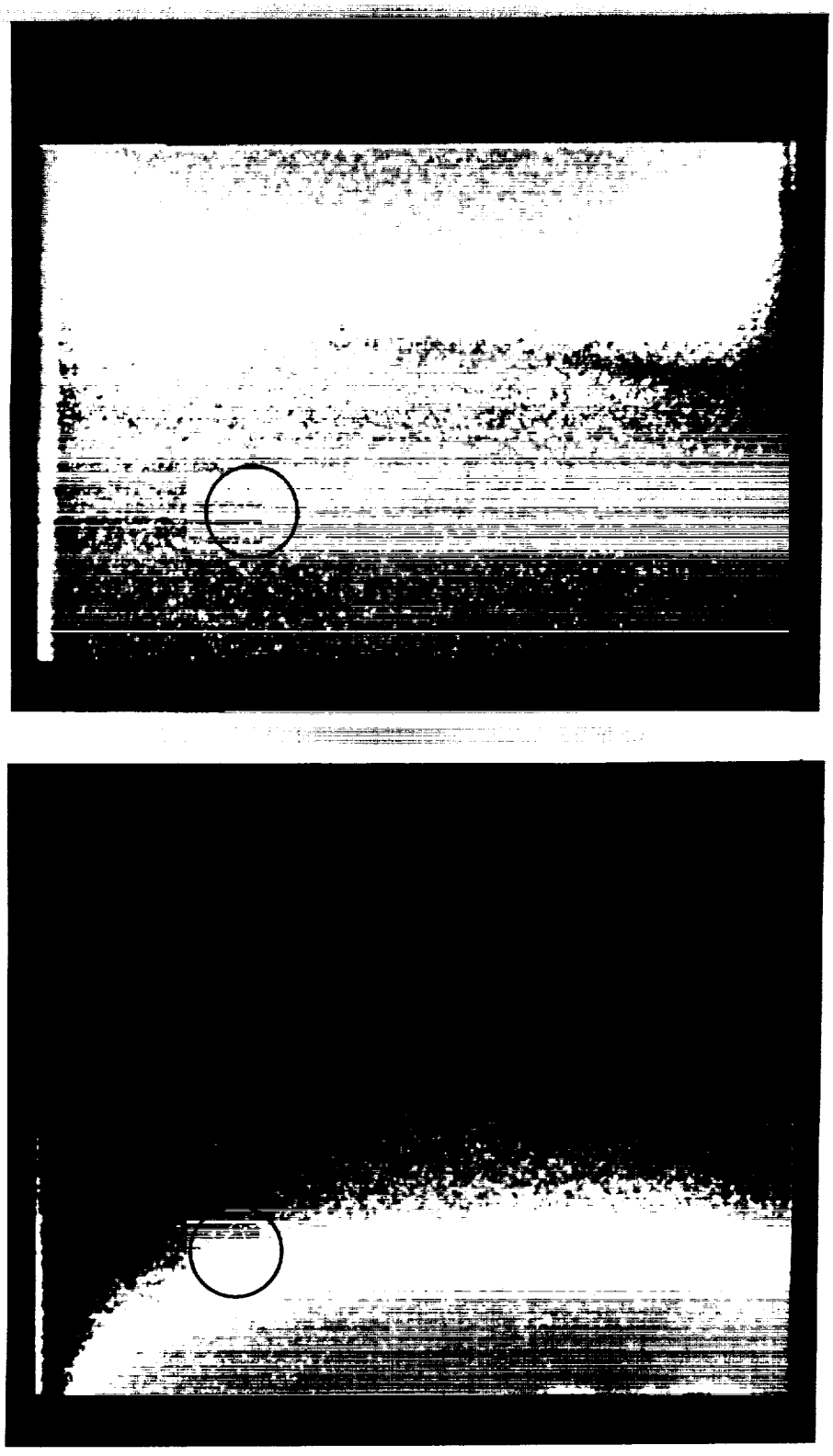

Figure 10. The two best candidates for "holes" in the 130.4-nm data set. (a) was taken on March 12, 1989 at 16:11 UT, and (b) was taken on December 24, 1986 at 21:58 UT. The candidate scan line intensity decreases are shown in the black circles.

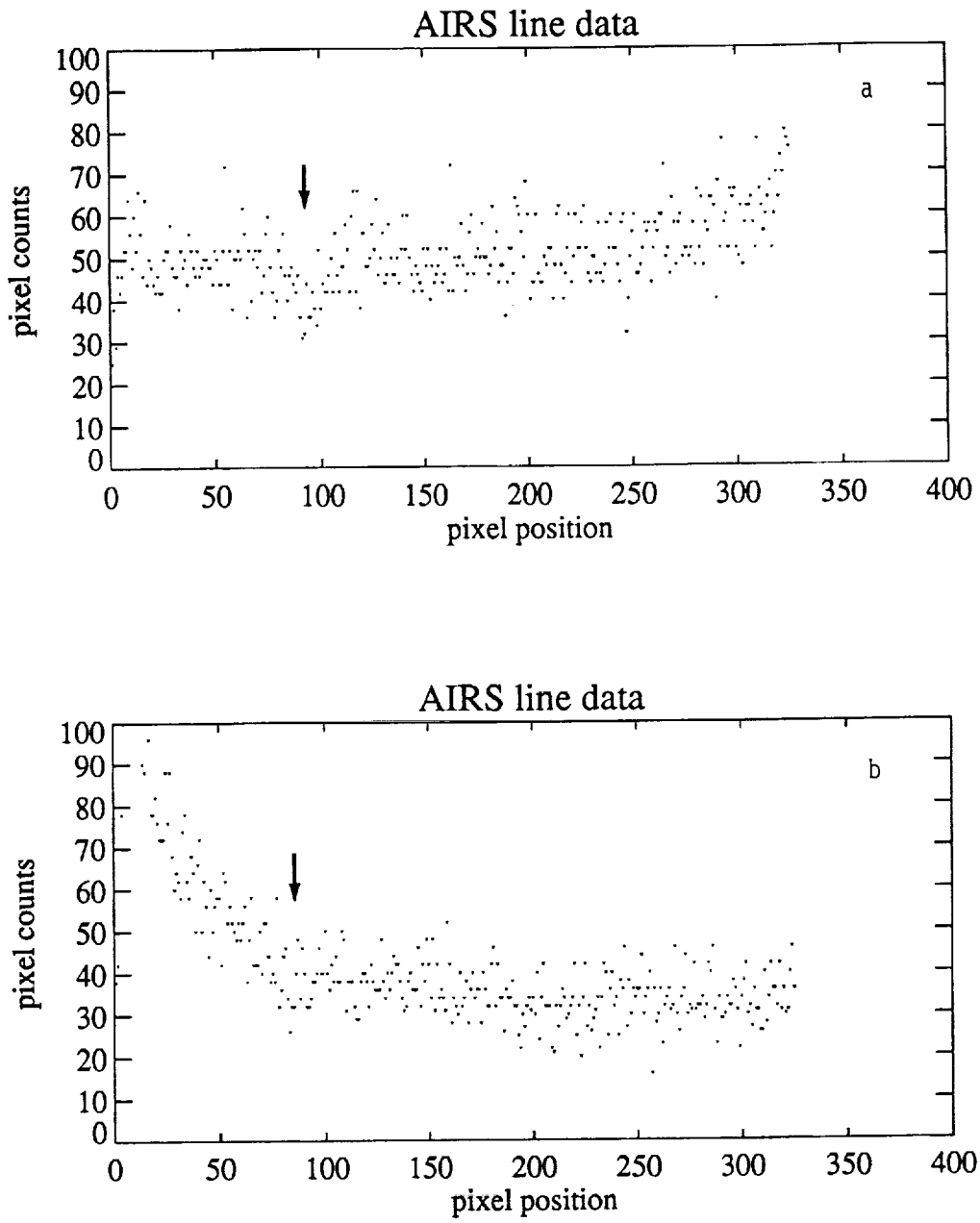

Figure 11. The pixel-count values (unpacked) versus the position along the scan line are shown for the previous two 130.4-nm candidates, where (a) is data taken on March 12, 1989 and (b) is data taken on December 24, 1986. An arrow indicates the pixel-count intensity decrease.

line numbers	83	84	85	86	87	88	89	90	91	92	93	94	95	96	97	98	99	100	101
71	52	38	56	48	44	44	46	46	52	50	48	46	56	46	48	52	58	48	50
70	60	48	42	46	42	48	48	48	46	52	56	48	56	40	50	44	44	42	46
69	46	46	40	46	50	44	36	44	44	40	52	46	52	52	62	62	52	52	40
68	48	50	52	50	30	60	50	56	44	56	38	40	46	46	48	44	40	42	58
67	46	48	38	50	40	40	42	40	44	46	48	52	42	42	42	38	56	60	46
66	56	50	52	44	56	56	52	64	58	48	52	44	40	64	48	50	38	56	52
65	40	56	50	30	46	62	48	42	48	60	52	44	44	50	48	52	50	62	50
64	60	40	44	48	52	50	48	36	58	58	48	46	56	48	42	58	44	30	52
63	38	50	56	56	38	68	52	52	66	42	60	50	48	52	48	52	60	40	50
62	46	40	46	48	44	42	46	36	31	32	44	36	36	42	38	34	52	38	44
61	40	40	50	48	50	44	52	52	52	42	40	56	44	52	52	50	70	48	52
60	56	50	38	50	38	52	42	50	34	48	42	60	40	50	44	30	42	52	64
59	52	46	46	52	42	48	48	46	60	58	44	64	34	60	36	50	44	46	38
58	52	44	52	52	48	50	52	46	52	44	50	50	50	48	48	40	56	42	56
57	50	56	50	52	50	42	52	48	46	44	38	48	46	50	46	40	42	60	52
56	60	38	60	46	68	40	44	36	56	44	38	52	52	44	50	48	50	56	50
55	48	62	44	52	42	48	62	44	46	50	50	48	42	48	48	52	40	50	52
54	52	52	48	46	38	48	64	46	56	62	48	46	42	48	52	56	52	56	52
53	44	44	52	52	48	42	50	42	56	42	48	42	38	52	46	52	42	44	50

pixel position on line

line numbers	76	77	78	79	80	81	82	83	84	85	86	87	88	89	90	91	92	93	94
70	46	52	58	52	50	52	48	44	42	44	60	56	50	46	44	38	46	50	40
69	66	64	38	50	44	42	68	56	52	40	52	44	56	36	50	48	44	48	52
68	38	42	48	48	46	44	44	44	48	34	46	48	62	52	36	50	42	44	60
67	62	38	40	50	46	46	52	42	38	52	58	40	58	52	42	42	52	48	52
66	56	42	52	46	46	62	38	40	68	48	44	42	52	44	46	36	50	44	44
65	52	46	42	44	52	32	46	56	52	38	56	64	34	56	48	44	50	48	40
64	48	58	38	48	38	42	38	48	32	42	46	40	42	42	44	50	48	48	48
63	46	42	40	50	32	34	32	58	42	42	40	44	50	36	46	36	38	48	46
62	58	38	50	42	56	50	52	62	52	40	40	44	52	40	48	36	48	46	40
61	38	58	32	36	44	46	34	26	32	32	40	48	34	46	40	32	32	34	38
60	56	44	48	46	34	56	56	40	48	52	42	48	58	46	50	52	46	32	29
59	46	50	46	42	44	30	46	36	40	48	40	48	36	38	40	46	40	44	31
58	50	58	42	38	38	52	34	52	52	40	34	38	48	44	34	36	42	44	46
57	30	42	34	42	46	50	42	58	48	36	48	42	38	42	50	40	34	44	32
56	34	36	40	32	32	36	40	32	44	38	44	50	40	40	36	34	34	36	40
55	40	32	32	36	34	34	32	42	46	44	32	48	52	52	36	46	56	38	40
54	42	38	42	38	50	40	34	38	29	36	38	42	38	38	38	52	28	38	40
53	52	34	40	40	46	40	44	34	42	48	32	44	42	46	40	40	34	38	29
52	40	46	36	52	44	42	34	40	42	48	44	38	42	42	32	32	44	44	32

pixel position on line

Figure 12. The actual counts of the pixel field for the 130.4-nm images shown in Figure 10, where (a) is data taken on March 12, 1989 and (b) is data taken on December 24, 1986. The pixel-intensity decrease is boxed in each case.

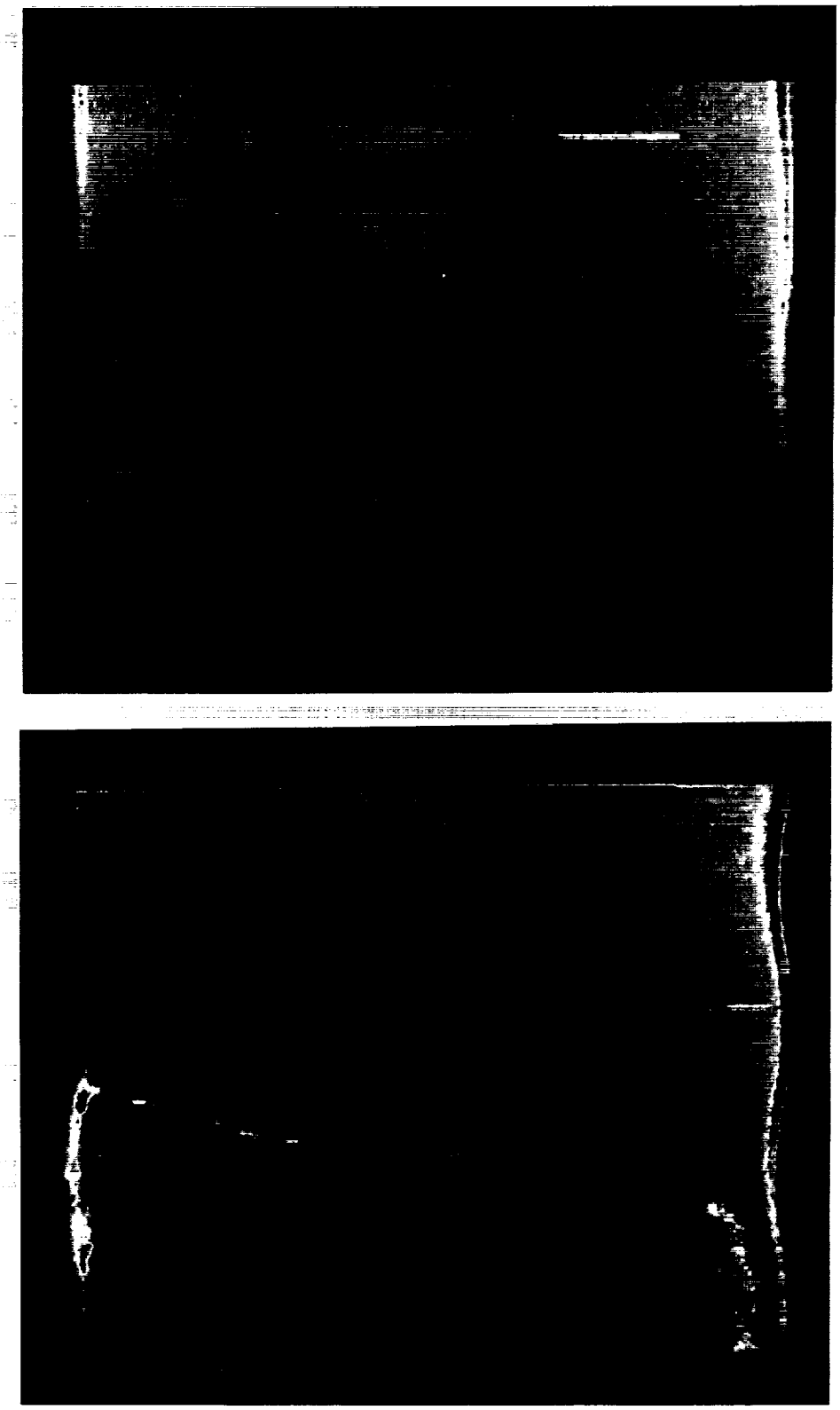

Figure 13. The two best candidates for "holes" in the 135.6-nm data set. (a) was taken on February 20, 1987 at 08:44 UT and January 30, 1987 at 10:32 UT. The candidate scan line intensity decreases are shown in the black circles.

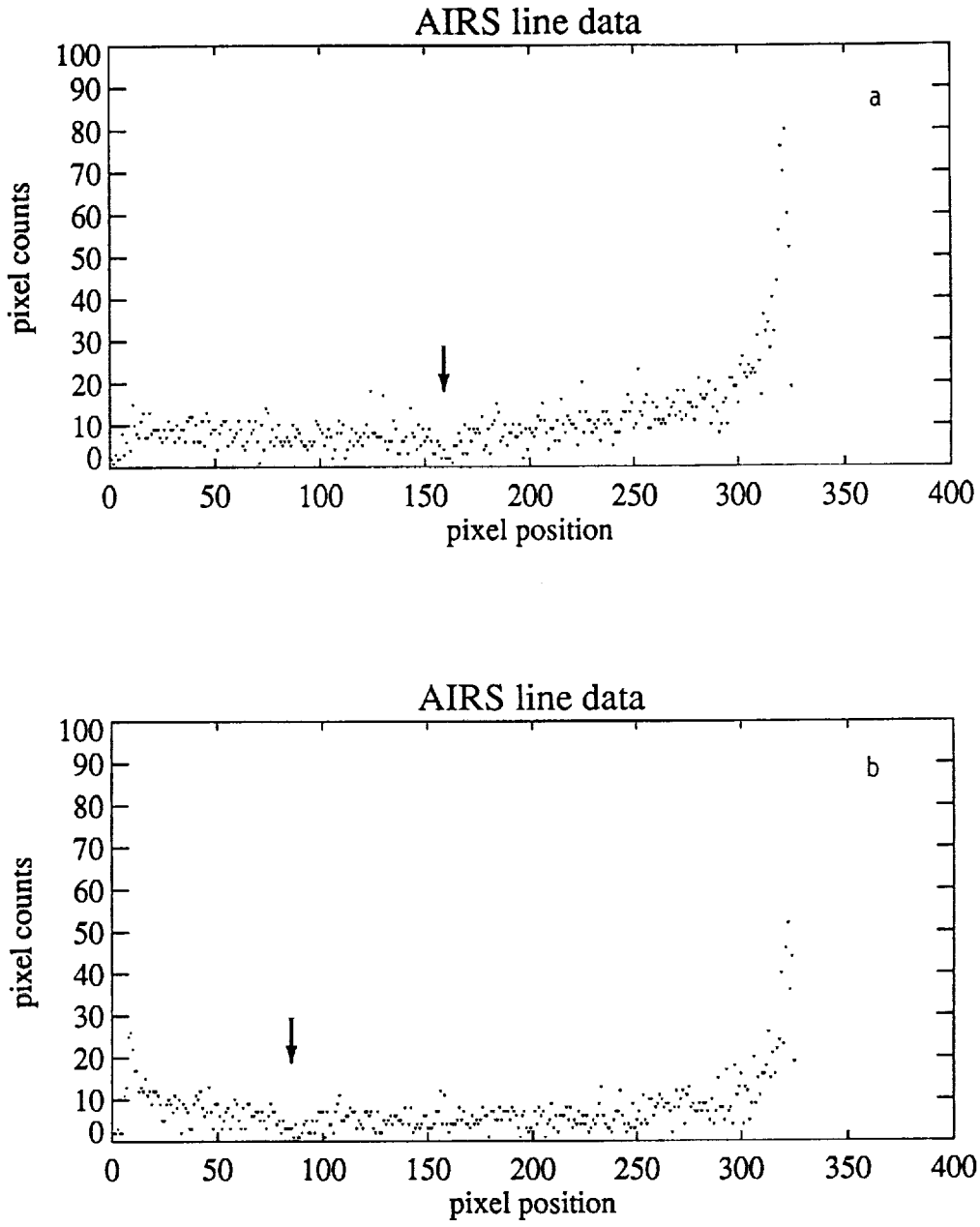

Figure 14. The pixel count values (unpacked) versus the position along the scan line are shown for the previous two 135.6-nm candidates, where (a) is data taken on February 20, 1987 and (b) is data taken on January 30, 1987. An arrow indicates the pixel-count intensity decrease.

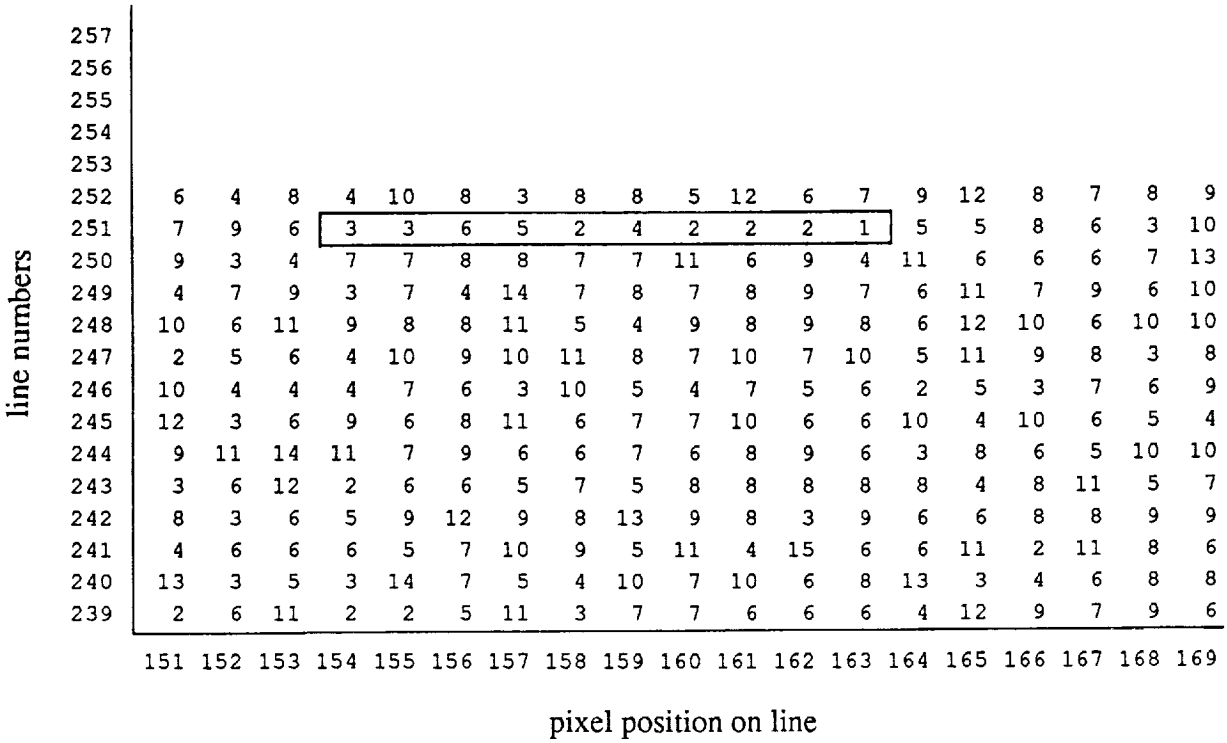

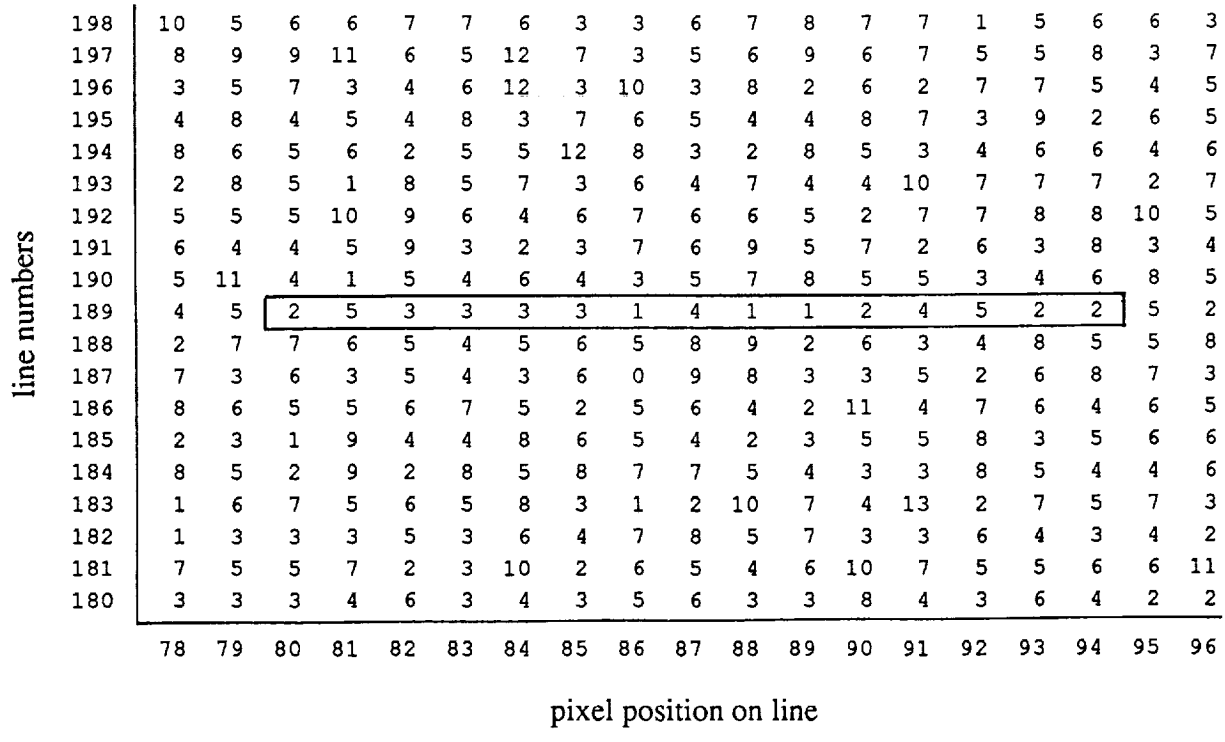

Figure 15. The actual counts of the pixel field for the 135.6-nm images shown in Figure 10, where (a) is data taken on February 20, 1987 and (b) is data taken on January 30, 1987. The pixel intensity decrease is boxed in each case.

Table 1. Summed-pixel values for the four "candidate" holes. "Line" and "pos." denote the central pixel location, "M" the number of pixels in each sum, "average" is the running mean of the outer six pixels, and "%" is the percentage ratio of the center sum to average value.

file	line	pos.	M	average	R	%	(summed values on scan line)						
pb306104	62	94	10	490.0	-5.20	76%	498	482	462	375	458	524	516
pb184836	61	85	15	691.5	-5.23	80%	914	806	682	554	602	563	582
pb225134	251	159	10	76.5	-5.32	39%	88	68	71	30	64	79	89
pb223918	189	87	15	90.2	-5.18	46%	116	94	93	41	83	84	71

V. DISCUSSION AND CONCLUSION

As indicated in Section II of this report, it was anticipated that about 0.11 "holes" should be observable in each full AIRS dayglow image when the hypothesized small-comet influx rate is at its average value of ~20/minute over the earth's surface. Unfortunately, although some of the AIRS data came from images with dayglow over most of the image, much of the AIRS dayglow data set was from partial dayglow images. The number of pixels in a full AIRS dayglow image should be about 300 (+/- 60 degrees along the scan line) by 200 (about 4000 kilometers along the ground track), for a total of approximately 60,000 pixels. Tables 2 and 3 show the sum (N) of pixel groups examined on a monthly basis for both 130.4 nm and 135.6 nm, using a grouping value of NGRP = 6 for Table 2 and NGRP = 4 for Table 3. The equivalent number (sum/60,000) of full dayglow images for each month from the accumulated data is also shown.

Table 2. The statistical data using M = 10 in Figures 6 and 7 binned into individual months. For each wavelength, the total sum (N) for the month is given, along with the number of full AIRS image frames to which this would be equivalent.

Month	130.4 nm	# images	135.6 nm	# images
January	975,277	16.3	908,297	15.2
February	129,262	2.2	1,880,470	31.3
March	138,781	2.3	625,120	10.4
April	0	0.0	16,135	0.3
May	1,372,730	22.9	0	0.0
June	0	0.0	0	0.0
July	258,346	4.3	0	0.0
August	0	0.0	0	0.0
September	0	0.0	0	0.0
October	0	0.0	0	0.0
November	741,322	12.4	181	0.0
December	1,413,230	23.6	5	0.0
Total	5,028,948	84.0	3,414,073	57.2

Table 3. The statistical data using M = 10 in Figures 8 and 9 binned into individual months. For each wavelength, the total sum (N) for the month is given, along with the number of full AIRS image frames to which this would be equivalent.

Month	130.4 nm	# images	135.6 nm	# images
January	1,072,060	17.8	957,011	15.9
February	108,630	1.8	1,969,700	32.8
March	130,307	2.2	596,089	9.9
April	0	0.0	13,324	0.2
May	1,503,730	25.0	0	0.0
June	0	0.0	0	0.0
July	280,799	4.7	0	0.0
August	0	0.0	8	0.0
September	0	0.0	0	0.0
October	0	0.0 0	0.0	
November	795,946	13.3	833	0.0
December	1,544,960	25.7	47	0.0
Total	5,436,432	90.5	3,537,004	58.8

As indicated by Figure 1 of Frank *et al* [1987a], there is some indication of a yearly variation in hole response rates in a manner similar to radar meteor rates reported by Vogan and Campbell [1957]. For January in particular, the number of holes observed decreased significantly, averaging about 1/3 the typical rate of 20/minute. December averaged about 2/3 the typical rate, and November averaged 1.5 times the typical rate. While May is not shown in Frank *et al* [1987], it can be extrapolated from Vogan and Campbell [1957] to be about the same as November (see Figure 6 of their paper). February and March appear to average about the same as January.

Using these monthly weighting factors on the data in Tables 1 and 2, and using only the 130.4-nm data, the total weighted equivalent full-dayglow images would be 79.7 for Table 1 and 86.7 for Table 2. The January and February monthly weighting values roughly balance the November and May monthly weighting values. Thus, in round figures, the weighted equivalent full-dayglow images from the hundreds of partial images is approximately 80 for the 130.4 data.

Unfortunately, essentially all of the 135.6-nm data were collected during the months of January, February, and March. Since these months showed rates about 1/3 the typical hole detection rate [Frank *et al*, 1987; Vogan and Campbell, 1957], the weighted equivalent full-dayglow images for the 135.6 nm data is slightly less than 20.

As noted by Dessler [1991], a paper by Meier [1987] indicated that 35% to 38% of the observed 130.4 emission has a last scattering above 300 km altitude. In the case of DE-1, that may not be critical (due to the higher observation altitude). In the case of AIRS data, this must be considered. If the hypothesized water-vapor cloud were detected at exactly 300 km altitude, the maximum decrease in intensity would be to 35% of the running average. Adding another

20% (the typical dark pixel value from Frank *et al* [1986]), the normal decrease in intensity should be about 50% of the running average. The majority of the cases detectable should be well above the 300 km altitude and thus should show far greater intensity reductions. As seen in Section IV, no event of even the 50% level of decrease was observed in the 130.4 nm data. The effect on the 135.6 nm intensity levels was not given in Meier [1987].

An additional effect that must be taken into consideration was mentioned in Frank *et al* [1989]. He noted that the total absorption cross section of H_2O has an absorption maximum near 130.4 nm and a broad absorption minimum centered about 144.0 nm [Watanabe and Zelikoff, 1953]. From Figure 1 in Watanabe and Zelikoff, [1953] it can be seen that the absorption coefficient at 135.6 nm is only about 50% of the coefficient at 130.4 nm. Unlike the Viking and DE instruments, the AIRS instrument is very discriminating in the VUV frequency being observed. Frank *et al* [1989] discussed the point of the relative ratios of 130.4 nm, 135.6 nm, and the N2 LBH bands. This ratio is not relevant in this study, but the relative absorption coefficient for 130.4 and 135.6 nm is quite relevant. We would not anticipate intensity reduction of atmospheric holes in 135.6 nm to be nearly of the reduction level found in the 130.4-nm data set. The combination of this effect and the relatively smaller amount of useable 135.6 nm data caused this study to concentrate on the 130.4 data set.

As described in the previous section, there was no case in the 130.4-nm data showing a pixel-string intensity decrease sufficient to be considered an atmospheric hole. Thus the probability that no hole would be observed in the full data set if the small-comet hypothesis is correct is equal to the probability that no hole is found in a full image, raised to the power of the total number of weighted equivalent full 130.4-nm dayglow images (set to ~ 80 above):

$$
\begin{aligned}
P(0) &= P(\text{no hole in image})^{(\#\ \text{full weighted images})} \\
&= ((1.0 - P(\text{hole in image}))^{(80)} \\
&= (1.0 - 0.11)^{80} \\
&= (0.89)^{80} \\
&\sim 1.0^{-4}.
\end{aligned}
$$

Thus the probability is extremely low that no intensity decreases indicative of an atmospheric hole would be observed in the 130.4 nm data set, if the small-comet hypothesis is correct. While there is a small degree of uncertainty in some of the assumptions in the calculation of the weighted equivalent full-image data, even if these estimates were decreased by a factor of 50%, the probability still would be $P(0) = (0.89)^{40} = 9.5 \times 10^{-3}$. We note that the total area of dayglow-image data at 130.4 nm is equivalent to 1.7 times the entire earth's surface. This suggests that the number of holes anticipated in the 130.4 data (~8.8) is a very conservative estimate with a hypothesized influx rate of 20/minute and a visibility duration of two to three minutes.

There are two cases in the 135.6 data that could be considered potential candidates for atmospheric holes. Given that the weighted equivalent full dayglow images for 135.6 nm was calculated to be slightly less than 20, a total of about $20 \times 0.11 = 2.2$ holes would be expected in the 135.6 nm data set. On the other hand, the two candidates do not show an intensity reduction

nearly as low as that observed in the holes observed at DE-1. In addition, the reductions are on the edge of the typical reductions expected of a Poisson distribution (due to the typically low 135.6-nm intensity levels). It is thus difficult to say that they are not, in fact, part of the expected Poisson distribution.

Another factor to note from Figures 6 to 9 is that as the grouping value, M, for the summed pixels decreases, an enhanced tail somewhat reminiscent of that in Figure 1 of Frank *et al* [1986] begins to appear. For the AIRS data these are known to be due to radiation-particle upsets to the counter for single pixels on board the Polar BEAR satellite. As the number of pixels in the group being summed decreases, the effect of a single anomalously low pixel is enhanced. Although the size and shape of this enhanced tail on the AIRS data distribution is not exactly like that of Frank *et al* [1986], its existence is suggestive.

While it is not possible to state definitively that the water-vapor clouds at the center of the small-comet hypothesis do not exist, especially given the somewhat ambiguous results from the 135.6-nm data set, this report presents strong evidence that they cannot have the characteristics required by that hypothesis. The probability that they would be missed (for the much larger 130.4-nm data set) in this search, given the characteristics that are required of the hypothesis, is considerably less than 1%. However, this is such an interesting and controversial hypothesis that further research may be warranted. Considerably better imagers are being planned for the next generation of satellites, and an analysis of their data should be both easier and more definitive.

REFERENCES

Cragin, B.L., "Comment on 'Search For Atmospheric Holes With the Viking Cameras' by L.A. Frank *et al*," *Geo. Res. Lett., 17*, 1173-1174, 1990.

Dessler, A.J., "The Small-Comet Hypothesis," *Rev. of Geophysics, 29*, 355- 382, 1991.

Frank, L.A., J.B. Sigwarth, and J.D. Craven, "On the Influx of Small Comets into the Earth's Upper Atmosphere I. Observations, II. Interpretation," *Geo. Res. Lett., 13*, 303-306, 1986.

Chubb, T.A., Comment to above paper, *Geo. Res. Lett., 13*, 1075-1077, 1986.

Cragin, B.L., W.B. Hanson, R.R. Hodges, and D. Zuccaro, Comment to above paper, *Geo. Res. Lett., 14*, 573-576, 1987.

Davis, P.M., Comment to above paper, *Geo. Res. Lett., 13*, 1181-1183, 1986.

Donahue, T.M., Comment to above paper, *Geo. Res. Lett., 13*, 555-557, 1986.

Hanson, W.B., Comment to above paper, *Geo. Res. Lett., 13*, 981-984, 1986.

McKay, C.P., Comment to above paper, *Geo. Res. Lett., 13*, 976-978, 1986.

Morris, D.E., Comment to above paper, *Geo. Res. Lett., 13*, 1482-1483, 1986.

Nakamura, Y. and J. Oberst, Comment to above paper, *Geo. Res. Lett., 13*, 1184-1185, 1986.

Rubincam, D.P., Comment to above paper, *Geo. Res. Lett., 13*, 701, 1986.

Soter, S., Comment to above paper, *Geo. Res. Lett., 14*, 162-163, 1987.

Wasson, J.T., and F.T. Kyte, Comment to above paper, *Geo. Res. Lett., 14*, 779-780, 1987.

Frank, L.A., J.D. Craven, K.L. Ackerson, M.R. English, R.H. Eather, and R.L. Carovillano, "Global Auroral Imaging Instrumentation for the Dynamics Explorer Mission," *Space Sci. Inst., 5*, 369-393, 1981.

Frank, L.A., J.B. Sigwarth, J.D. Craven, Reply to Chubb's Comment, *Geo. Res. Lett., 13*, 1079-1082, 1986.

Frank, L.A., J.B. Sigwarth, J.D. Craven, Reply to Soter's Comment, *Geo. Res. Lett., 14*, 164-167, 1987a.

Frank, L.A., J.B. Sigwarth, J.D. Craven, Reply to Cragin *et al's* Comment, *Geo. Res. Lett., 14*, 577-580, 1987b.

Hunt, J.W., and C.E. Williams, "Anomalous Attitude Motion of the Polar BEAR Satellite," *Johns Hopkins APL Technical Digest, 8*, Number 3, 324-328, 1987.

Frank, L.A., J.B. Sigwarth, and J.D. Craven, "Search For Atmospheric Holes with the Viking Cameras," *Geo. Res. Lett., 16*, 1457-1460, 1989.

Kerr, R.A., "Double Exposures Reveal Mini-Comets?" *Science, 243*, 170-171, 1989.

Meier, R.R., "Issues Relating to "Holes" in the OI 1304A Far UV Dayglow," *Planet. Space. Sci., 35,* 1297-1299, 1987.

Schenkel, F.W., B.S. Ogorzalek, R.R. Gardner, and R.A. Hutchins, "Simultaneous Multi-Spectral Narrow Band Auroral Imagery from Space (1150A-6300A)," *SPIE Ultraviolet Technology,* 90-103, 1986.

Schenkel, F.W., and B.S. Ogorzalek, "Auroral Images from Space: Imagery, Spectroscopy, and Photometry," *Johns Hopkins APL Technical Digest, 8,* No. 3, 308-317, 1987.

Vogan, E.L. and L.L. Campbell, "Meteor Signal Rates Observed in Forward-Scatter," *Canad. J. Phys., 35,* 1176-1189, 1957.

Watanabe, K. and M. Zelikoff, "Absorption Coefficients of Water Vapor in the Vacuum Ultraviolet," *J. Opt. Soc. of Am., 43,* 753-755, 1953.

Yeates, C.M., "Initial Findings From a Telescopic Search for Small Comets Near the Earth," *Planet. Space Sci., 37,* 1185-1196, 1989.

NASA

Report Documentation Page

1. Report No.	2. Government Accession No.	3. Recipient's Catalog No.

4. Title and Subtitle
Report on the Search for Atmospheric Holes Using AIRS Image Data

5. Report Date
13 December 1991

6. Performing Organization Code

7. Author(s)
Lee A. Reinleitner, Ph.D.

8. Performing Organization Report No.
NWRA-CR-91-R074

10. Work Unit No.

9. Performing Organization Name and Address
Northwest Research Associates, Inc.
P.O. Box 3027
300 120th Avenue N.E., Bldg. 7, Ste. 220
Bellevue, WA 98009

11. Contract or Grant No.
NASW-4535

13. Type of Report and Period Covered
Final
9/27/90 - 9/26/91

12. Sponsoring Agency Name and Address
NASA Headquarters
Washington, DC 20546

14. Sponsoring Agency Code

15. Supplementary Notes

16. Abstract

Frank *et al* [1986] presented a very controversial hypothesis which states that the earth is being bombarded by water-vapor clouds resulting from the disruption and vaporization of small comets. This hypothesis was based on single-pixel intensity decreases in the images of the earth's dayglow emissions at vacuum-ultraviolet (VUV) wavelengths using the DE-1 imager. These dark spots, or atmospheric "holes," are hypothesized to be the result of VUV absorption by a water-vapor cloud between the imager and the dayglow-emitting region. This report examines the VUV data set from the Auroral Ionospheric Remote Sensor (AIRS) instrument that was flown on the Polar BEAR satellite. AIRS was uniquely situated to test this hypothesis. Due to the altitude of the sensor, the holes should show multi-pixel intensity decreases in a scan line. A statistical estimate indicated that sufficient 130.4-nm data from AIRS existed to detect eight to nine such holes, but none was detected. The probability of this occurring is $< 1.0 \times 10^{-4}$. A statistical estimate indicated that sufficient 135.6-nm data from AIRS existed to detect ~2 holes, and two ambiguous cases are shown. In spite of the two ambiguous cases, the 135.6-nm data did not show clear support for the small-comet hypothesis. The 130.4-nm data clearly do not support the small-comet hypothesis.

17. Key Words (Suggested by Author(s))	18. Distribution Statement
atmospheric holes small comets dayglow vacuum ultraviolet VUV	

19. Security Classif. (of this report)	20. Security Classif. (of this page)	21. No. of pages	22. Price
Unclassified	Unclassified	31	

NASA FORM 1626 OCT 86